

## 2.6 Seismic Applications (SEI)

The Seismic research area has had a tremendously successful year with emphasis on analysis of data captured by the Middle America Seismic Experiment (MASE), redeployment of the equipment in the Peru Subduction Zone Experiment (PeruSZE), and successful completion of the Reftek ENSBox platform for both structural and seismic applications.

### MASE and PeruSE

Our cross-Mexico wireless network, MASE, was dismantled in early 2007 and after repairs and refurbishment, the equipment was shipped to Peru to do a similar experiment, PeruSze, across the Andes where the Nazca plate is subducting beneath the west coast generating devastating earthquakes and tsunamis. Graduate and undergraduate students were involved in the installation of the 49 station network over the summer. Most stations at the end of the summer were recording on-site. Subsequently Richard Guy and Igor Stubailo have installed the networking that links the stations across the Andes. The experiment will run for one or two more years. P. Davis will take a class there to do geophysics in May.

The Peru experiment (field work funded by the Caltech Moore Foundation grant) provided an opportunity to redesign our networking protocols based on our 2-year networking experience in Mexico. Our Delay Tolerant Shell (DTS) was improved. A new website for hourly system status was designed and implemented. The data was input to LabView. The various synergies of CENS have combined to make a significant remote area networking product. The data is radioed across Peru to Internet drops. It is then transmitted to UCLA over the Internet. The Atacama desert, where the network is located, is one of the more remote parts of the world. The facility that has been developed to install a remote wireless network over 250 km, and have the data transmit back to the laboratory, as well as duplex control on the instrumentation in the field, has application worldwide where remote network sensing is required.

### CENS Development of the Reftek EnsBox with application to GeoNet-SHMnet-ShakeNet-FlexiRAMP

What does this acronymic soup have in common? The short answer is CENS. CENS has provided the infrastructure and technology to link half a dozen departments in a single development with an industrial partner (Reftek Refraction Technology of Plano Texas). It is the culmination of our experience in wireless networking to design a node that satisfies the digitizing and wireless networking requirements of the following groups to improve their science:

- **GeoNet** (geophysical monitoring) Paul Davis, Department of Earth and Space Sciences, UCLA, earthquake and tectonic networks.
- **SHMnet** (Structural Health monitoring) John Wallace, Civil Engineering, UCLA
- **ShakeNet** (Monitoring civil structures for shaking after earthquakes) Monica Kohler, CENS and Caltech, Ramesh Govindan, USC, Department of Computer sciences
- **FlexiRAMP**, A flexible network for Rapid Array Mobilization Procedures, IRIS (Incorporated Research Institutions for Seismology) Richard Allen Berkeley, Marcos Alvarez, IRIS, and Paul Davis, UCLA. {in association with Deborah Estrin, CENS, Computer sciences, UCLA and Bill Kaiser, Electrical Engineering, UCLA}

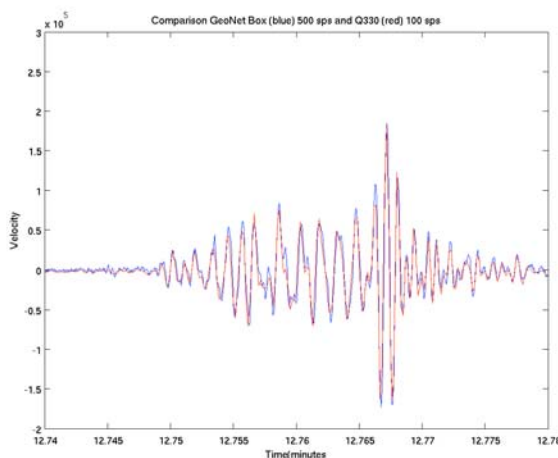


Figure 4. Prototype Reftek EnsBox for GeoNet, SHMnet ShakeNet and FlexiRAMP applications. MEMS seismometer on left. Shielded Circuits include TI A/D, UCLAs LEAP or Crossbow Imote II processor board. Wireless 802.11b card.

The idea of an 'EnsBox' dates back to our CENS retreat in Palm Springs, 2006, where domain, computer, and electrical engineering scientists broke out into design groups to chart the future of CENS developments that would have greatest impact. Among others, the specification of an EnsBox emerged.

For GeoNet and FlexiRamp, the science objective is to use a rapidly installable wirelessly linked seismic network to make near-real time unaliased observations in aftershock or volcanic zones in RAMP deployments or in structures.

The immediate technical objective involved collaborating with Reftek to construct a new generation digital acquisition system (DAS) based on the CENS-developed LEAP (low-power energy aware processing) system and a newly developed low-power A/D converter from Texas Instruments (TI) that became available last year. By using the processor in low power mode for data acquisition, and moderate-power mode for on-site analysis and wireless transmission we reduce infrastructure for nodes, so that, in theory, hundreds can be deployed rapidly and self configure. Costs for the prototype were shared by CENS and NEES (John Wallace's group) who are interested in structural health monitoring (SHM). We used the Mexico and Peru networks to field-test software including improving Disruption Tolerant Shell (DTS), measurement of radio link quality (ETX), improved network logging, a Web interface based on Emstar for deployment and maintenance, network time, a new routing protocol that caches the routes across sleep cycles for a fast startup. Reftek president Paul Passmore and head engineer Phil Davidson have visited UCLA and USC on four occasions since beginning of development. At the last visit (13 Feb, 2009), they brought prototype boxes. A prototype (Figure 4) was displayed at the Earthscope meeting 2008. A one day workshop on FlexiRAMP is supported by IRIS at the Seismological Society of America in Monterey April 7. The Reftek EnsBox will be featured. This meeting is preliminary to an anticipated IRIS MRE application to NSF for a FlexiRAMP national pool of equipment. If the Reftek EnsBox is chosen it will be a satisfying outcome for the CENS development.

The Seismology research area's productive year can be clearly seen in the accomplishments of its students and faculty. Martin Lukac received his PhD, Allen Husker was appointed a faculty member at UNAM, Derek Skolnick defended his PhD and was employed by Kinematics. Antonio Dominguez, a Mexican student, funded by the Mexican Government, will take his PhD qualifying exam based on the Mexico data collected by CENS. Several papers have been published both on the computer and Earth science applications including one in Science (Song et al., 2009). Igor Stubailo won an Outstanding Student Paper award from the Seismological Society of America. We took a UCLA geophysics class combined with Caltech to conduct a gravity survey across the Andes in Peru. Our PeruSE seismic network recorded the M=8.8 earthquake. With ~100 stations it is the largest nearby network to record such a giant event. We held an IRIS-sponsored FlexiRAMP workshop. We successfully tested the GeoNet box in the Mojave Desert. The shakeNet box (its twin) was successfully used in a building test. Forty units have been ordered from Reftek. More details can be found in the extended report.

# SEI 01 Peru Seismic Experiment Tomography and Gravity Inversion

## SEI 01.1 Overview

The Peru Subduction Experiment (PERUSE) is a collaborative project developed by UCLA, Caltech, the French L'Institut de Recherche pour le Développement (IRD) and Instituto Geofísico del Perú (IGP) to improve geophysical models of the Andean Orogenic Belt and to image the subduction process in Southern Peru. One area of particular interest is where the Nazca Plate transitions from a normally subducting slab at an angle of about 30° to a shallow subducting slab beneath the South American Plate.

The PERUSE project, which started in the summer of 2008, consists of a linear array of 50 broadband seismic stations that are evenly spaced about 6 kilometers apart. They are aligned perpendicular to the coast of Peru, from Mollendo to Juliaca. Caltech deployed 50 more stations during 2009. Their line runs perpendicular to the current line, from Juliaca to Cusco. By the end of 2010, a third linear array will be installed north of and perpendicular to Caltech's line in the Altiplano. The current UCLA/CENS line is located in a region with steeper subduction while the Caltech line is approximately located over the transition zone of flat and steep subduction. The third line from Cusco to the coast will be used to study the region with shallow subduction.

## SEI 01.2 Approach

The PERUSE project, which started in the summer of 2008, consists of a linear array of 50 broadband seismic stations spanning approximately 300 km. The 50 seismic stations are wirelessly linked using 802.11b to collect the data in near real time and provide information about the health an operation of the network and each station. The deployment of the first line was completed in January 2009 and the second line was completed in December 2009.

## SEI 01.3 Accomplishments

We have processed a subset of the data collected for local events. We have also developed an event detector to identify local earthquakes and pick the p-wave arrivals. We used hypo71 to locate the earthquakes. Preliminary results from gravity measurements indicate that the crustal root of the Andes dips approximately 20° on both sides of the range, and extends to a depth of approximately 70km. This also agrees well with the receiver function results, which show that the crust thickens from the coast of Mollendo through the Altiplano to Juliaca to a depth about 70km (Phillips et al, Fall AGU 2009). Teleseismic studies also indicate that the crustal thickness varies laterally below southern Peru. We developed simple tomographic model that indicated the depth to the Moho is 80km. Also, the Moho depth mirrors the topography and is generally consistent with the gravity results. Our results indicate that the Moho rises East of the Western Cordillera and may exhibit similar behavior beneath the Eastern Cordillera.

## SEI 01.4 Future Directions

We are developing a heterogeneous 2-dimensional model from the topographic and gravity data, teleseismic events, and the receiver function results to accurately locate earthquakes in the area of interest and to provide a better crustal model of the region. We also plan to develop a complete 3-dimensional tomographic model of the Andean Mountains and the subduction zone beneath Peru which will include the slab. We will also use our data to do SKS

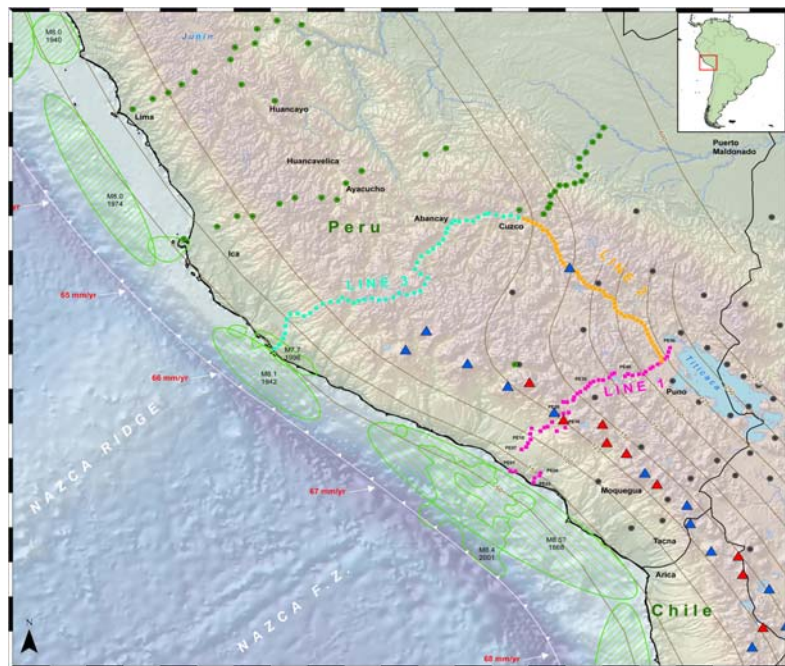


Figure 1. The current deployment consists of two lines, line 1 (pink) and line 2 (orange). The UCLA CENS line, in pink, spans from Mollendo on the coast, over the volcanoes surrounding Arequipa, and across the high desert to Juliaca near Lake Titicaca. The Caltech line, in orange, spans from Juliaca to Cusco. Line 3, in light blue, will be deployed by the end of summer 2010.

splitting and Surface Wave Tomography. We will continue locating local earthquakes with our network and create an improved version of IGP's catalog of local events.

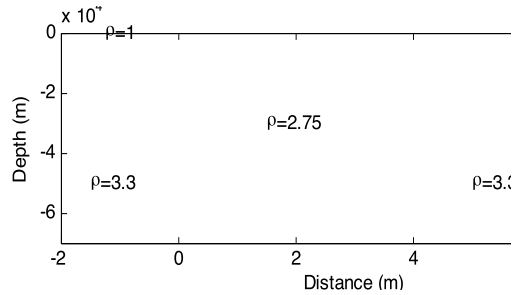


Figure 2. Upper plot: Bouguer gravity survey (red stars) fit to the gravity signature generated by the Talwani model (blue stars) of the region. Bottom plot: Talwani polygon model. We assumed a mean density of the ocean to be 1.0 g/cm<sup>3</sup>, a mean density of the crust to be 2.75 g/cm<sup>3</sup>, and a mean density of the mantle to be 3.3 g/cm<sup>3</sup>. Based on isostasy, the high elevations of the Andean Altiplano should be mirrored in the Earth's interior by a crustal root in the mantle.

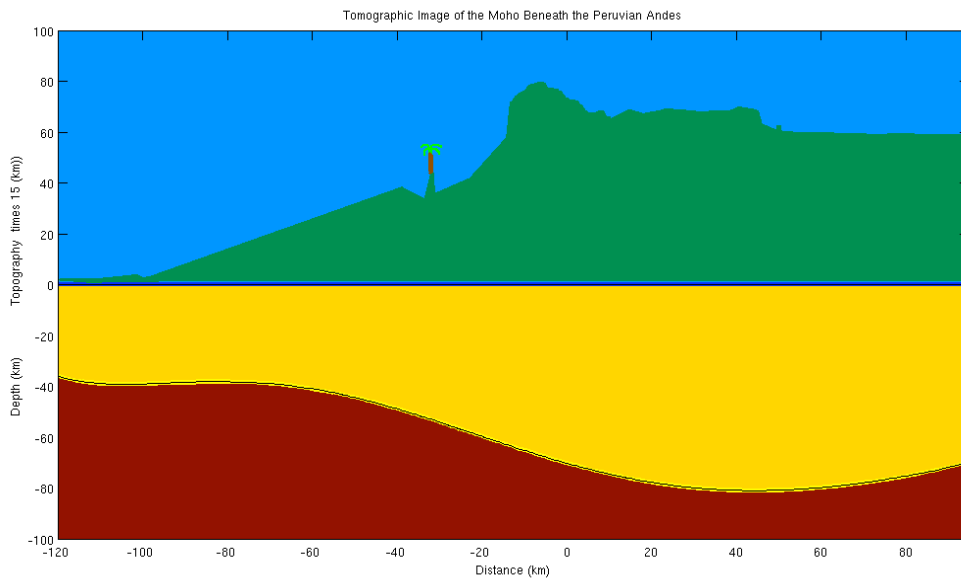


Figure 3. Back projected tomographic image of the crust and mantle beneath the Peruvian Andes. We fit the data to a 6th order polynomial to get the smooth curve for the Moho beneath the Andes. Our simple tomographic model indicates that the Moho reaches to a depth of 80km beneath the Andes. Our results also indicate that the root begins to recover to the east of the Andes.

## SEI 02 Surface wave analysis of MASE data and integration with other experiments

### SEI 02.1 Overview

We present azimuthally anisotropic fundamental mode Rayleigh wave phase velocity maps for the Mexico area. Body wave tomography in this region reveals the presence of a flat slab under the western part of the MASE seismic array (which ran from Acapulco to Tampico), starting at about 30-50 km depth, and of a steeply dipping slab beneath the center of the array. In addition, preliminary shear-wave splitting (SKS) results in the region did not show any significant difference between measurements made above the slab and away from it. While these SKS splitting observations need to be further refined with stacking, our anisotropic phase velocity maps will help put them in context and constrain the depth of origin of the anisotropy. In this study, we analyzed data recorded at 100 broadband stations (MASE array) installed from Acapulco to Tampico in Mexico over a period of 1.5 years and 38 permanent Mexican stations for 155 teleseismic events of magnitude 6.0 and above. We employed a two station method to measure phase velocity dispersion curves between periods of 20 to 170s, using events located within 3 degrees of the great circle path between the two stations. Considering that Rayleigh waves at 170s are sensitive to shear-wave velocity structure down to about 300 km, this should enable us to reveal the upper part of the slab.



Figure 1

### SEI 02.2 Approach

A 100-station broadband array (the Meso-American Subduction Experiment or MASE array) was deployed during 2005–2007 across central Mexico. The array extended from Acapulco on the Pacific coast to Tempoal, near the Gulf of Mexico in the north, passing through Mexico City. The network contained 50 traditional stand-alone seismic stations and 50 wirelessly connected sites. The data collection and delivery software for the wireless network was developed at CENS.

For this study we used MASE data as well as data collected by the permanent Mexican Servicio Sismológico Nacional (SSN) network.

### SEI 02.3 System(s) Description and/or Experiments

The analysis procedure is a two-station method developed by Snoke and his colleagues, based on developments made by Herrmann (1987), to determine inter-station dispersion phase velocities. One of its big advantages is that if the two stations share a common great-circle path, the deconvolution of the near-station waveform from the far-station waveform at least in principle removes the effects on the calculated dispersions of the Earth structure between the epicenter and the near station. A limitation is that one is restricted to earthquakes and station geometries that fit the selection criteria. However, the dense network of MASE and SSN stations (~5 km and ~50 km spacing, respectively) means that there are many suitable station pairs for earthquakes with a wide range of magnitudes and epicentral distances. Our general study area is a good distance from several regions with large earthquakes that produce clean waveforms at these stations. Fig. 2 shows the location of the events selected for our Rayleigh wave analysis and Fig. 3 shows the ray coverage obtained. For each earthquake, we identify pairs of stations with difference between the backazimuths of the far station to the epicenter and to the near station smaller than 3°. We then process the seismograms for all these stations by correcting for the (known) instrument response, decimating to

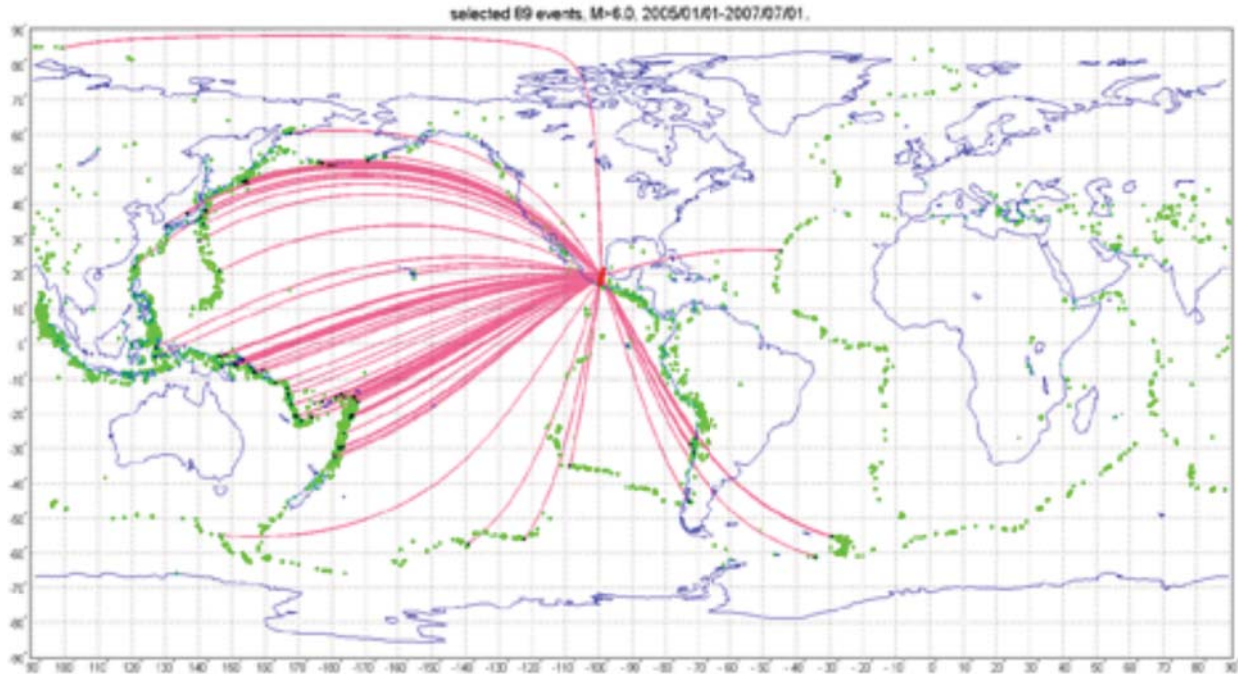


Figure 2

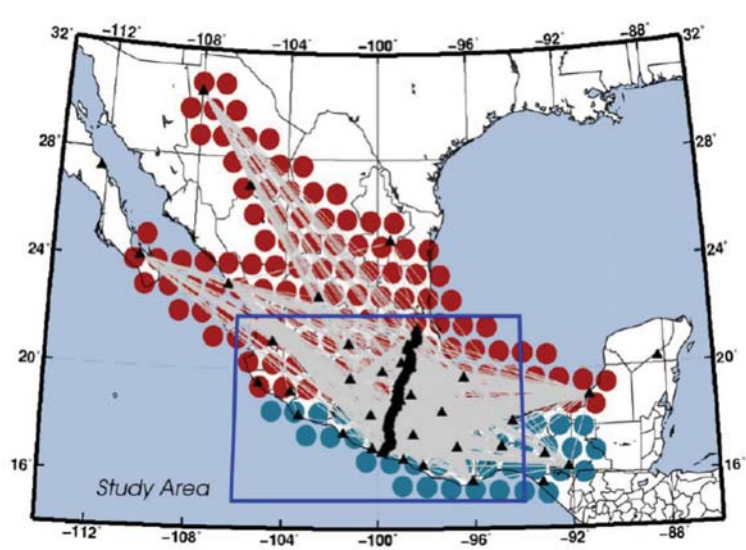


Figure 3

1 sps, and integrating to displacement. Next, we use a frequency-time analysis (FTAN) (Dziewonski et al., 1969; Landisman et al., 1970) on a representative subset of stations to identify the appropriate range of group velocities for each event and to check on the quality of the group-velocity spectrum.

Examples of FTAN analysis are shown in Fig. 4. In both cases, the two stations are approximately along a common GCP (within 3?). For both stations, the group-velocity plots are well behaved (smooth contours over most of the targeted period range) at periods between 16s and 170s. If the FTAN plots are not well behaved, we reject at least those stations and perhaps the event. Causes of bad FTAN plots could be small magnitude, complicated source function, paths that cross one or more tectonic boundaries at sharp angles leading to a bend in the wavefronts or severe multipathing.

For each selected station pair, we obtain the phase velocities across the frequency band of interest with a single set of computations by calculating the inter-station Green's function in the frequency domain. The standard deviation in

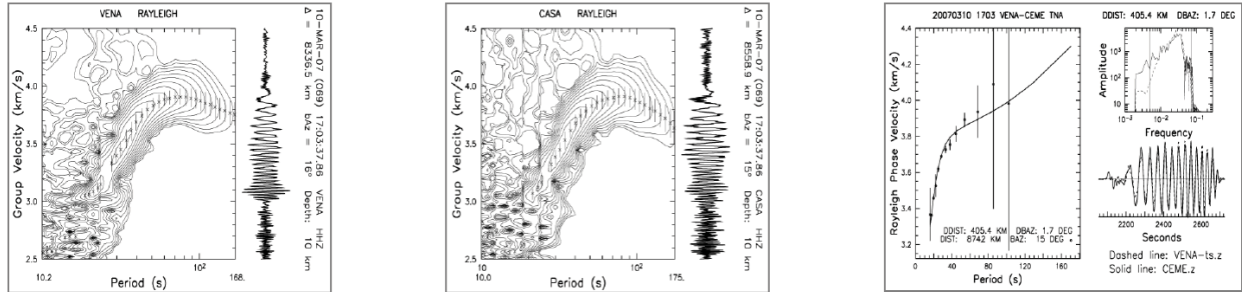


Figure 4

phase velocity is estimated at each frequency, based on the coherency of the two waveforms after the near-station record has been timeshifted to the far-station time using the calculated phase velocities (see Warren et al. (2008) for details). The frequency range at which dispersion curves can be determined depends on the inter-station distance. As a rule of thumb, the ideal station spacing should be at least the wavelength of the longest period analyzed and always greater than 1/2 wavelength (e.g. at a period of 150s the wavelength of a phase traveling at 4.4 km/s is 660 km; at 20s a phase velocity of 3.6km/s corresponds to a wavelength of 72km). A station spacing of 600 to 1000km is thus ideal to measure the longest periods and to get information on the deep upper mantle (~200 km depth). Shorter inter-station distances will give better short period analyses, which will help constrain the shallow upper mantle.

After calculating the phase velocities, we invert them and obtain phase velocity tomographic maps, like in Fig.5, which are interpreted with sensitivity curves.

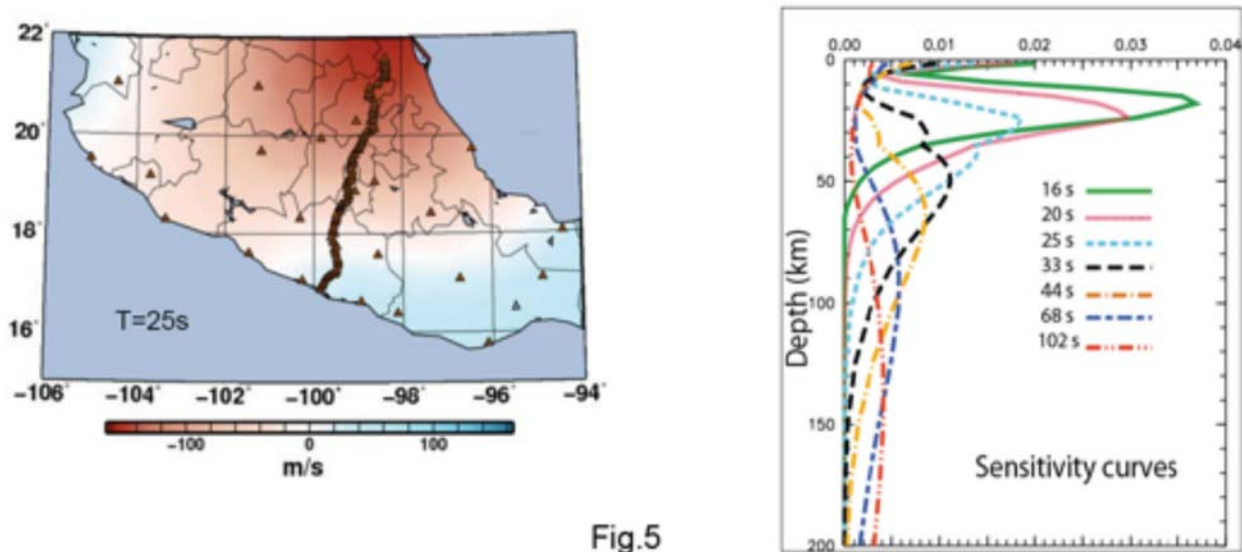


Fig.5

#### SEI 02.4 Accomplishments

We obtained phase velocity maps for Mexico region and identified the subducting slab with Rayleigh wave velocities. We can clearly see the contrast between the fast and slow velocities where the slab is dipping as shown in Fig.6

The results were presented at the 2009 Fall Meeting of American Geophysical Union in San Francisco during oral presentation.

#### SEI 02.5 Future Directions

Our surface wave analysis indicates an increase in phase velocities in the period range of 25 to 65 s going from the SW to the NE end of the transect, indicating the presence of the slab. The estimated minimum slab thickness (~60 km) and the location of the change in phase velocity approximately match previous results from P-wave tomography. This method can be used easily in other areas to identify the velocity anomalies.

In the future we would like to improve our analysis by stacking of signals from different events at the stations of interest. In addition, we will invert the measured path-averaged dispersion curves to model the depth-dependence of

the velocity structure within the upper part of the slab. We will compare and combine our results with those from previous studies. We also would like to invert the phase-velocity maps to obtain the 3D velocity structure and 3D anisotropy of the region to see the depth's velocity values.

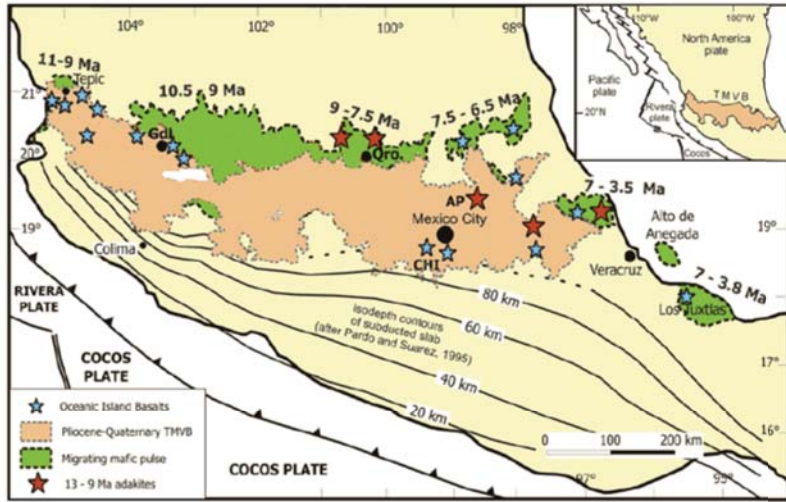
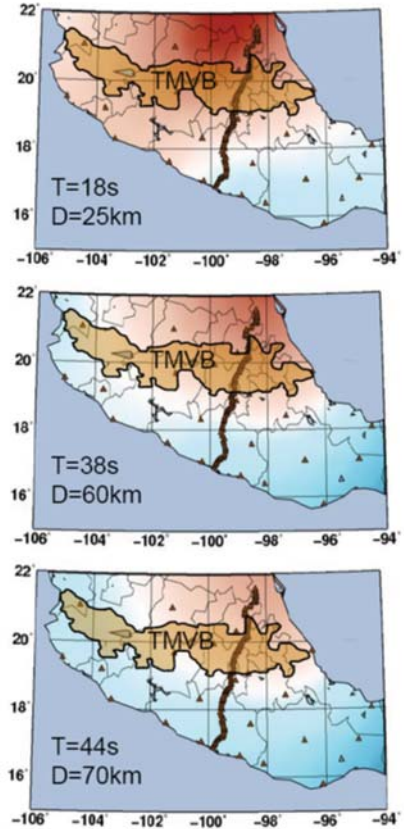


Fig.6



## SEI 03 Microseisms interpreted as coastal reflections of ocean waves generated by storms based on Mexico Array data

### SEI 03.1 Overview

We are exploring the correlation of daily microseism travel times, amplitude, and azimuth along the linear MASE seismic array with global wave height and global sources of microseisms. The Meso-American Subduction Experiment (MASE) was a 100 station 500km linear broadband seismic array deployed for 2 years across Mexico. The time series of daily travel times between pairs of stations, determined from noise correlation, fluctuates by up to two seconds, and are correlated with one another across independent pairs of nearly aligned stations. We have successfully modeled the fluctuations between stations by describing the phase change introduced by the biased energy from the off receiver-line sources. The goal of this effort was to enable the application of Data Driven Time Synchronization (DDTS), which uses underlying characteristics in the data to provide time synchronization, to repair incorrectly time synchronized data. The method was successful.

To further improve the accuracy of seismic DDTS we began searching for an external model to correlate the travel time fluctuations with. Part of this model is determining where precisely the microseism are generated. The search has uncovered new correlations between global ocean effects such as wave height and helped us develop a model based on these correlations which can predict the microseism travel time fluctuations. This model supports the theory that for our array, microseisms are generated near the Mexican coast and not in the southern hemisphere as was generally believed before.

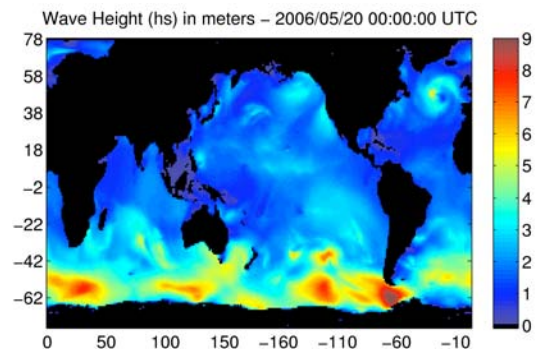


Figure 1. Sample wave height output from WAVEWATCH III. We used ocean effect outputs to develop external models to predict the microseism travel times.

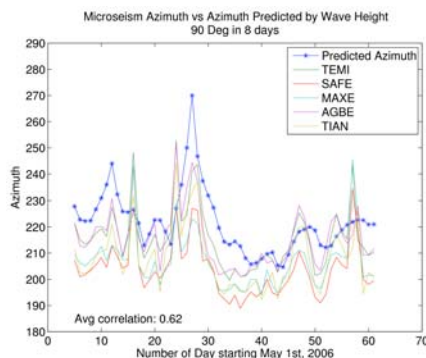


Figure 2 Microseism azimuth computed from the wave height shown with the microseism azimuth computed from the seismic data.

### SEI 03.2 Approach

There are two prevailing theories on the sources of microseisms for our network. They do not differ in how the microseisms are created but they differ in where microseisms are created relative to the stations. Both theories describe microseisms generated in interfering ocean surface waves. The first, which we will call the  $\Psi_c$  theory, proposes that the microseisms come from storm centers, specifically the Roaring Forties, the storms in the lower southern latitudes.  $\Psi_c$  is the microseism source intensity: it is the expected amplitude of the microseisms at the source. The second theory, which we will call the HR theory, proposes that the microseisms are generated by the ocean waves from the storms in the Roaring Forties, but after the waves have traveled to and reflected off of the coast. In other words, the coastal reflection interferes with the incoming ocean surface waves in the correct way to create microseisms. This occurs within 5000Km (about 45°s of latitude) of the stations. In this case, the effects from the storms are essentially delayed by the amount of

time it takes for the ocean surface waves to travel from the storm to the coast. Both of these theories can be tested and verified using existing data sets of weather and ocean effects: wind velocity, wave height, and the microseism source intensity ( $\Psi_c$ ).

Using the weather and ocean effects we searched for an external model to correlate our results to and potentially track the microseisms over time. Our search has focused on the global wave height, wave-wave interaction intensity ( $\Psi$ ), and microseism source intensity ( $\Psi_c$ ) and we correlated these with the measured microseism azimuth, microseism amplitude, and microseism travel time.

### SEI 03.3 System(s) Description and/or Experiments

We began with two month time series (on a one day scale) of microseisms azimuth, microseism amplitude, and microseism travel time and used various methods for correlation. To test the  $\Psi_c$  theory we used the ocean effects from the entire planet over the same two months. We obtained these by running the National Oceanic and Atmospheric Administration (NOAA) / National Centers for Environmental Prediction (NCEP) WAVEWATCH III wave

action model software. To test the HR theory we followed the same processes except restricted the search regions near the coast of Mexico.

### SEI 03.4 Accomplishments

Our search revealed two strong correlations. When restricted to a 5000Km region around our array, we can correlate the ocean wave height with the microseism azimuth and the microseism amplitude. Figure (2) and Figure (3) shows these correlations. With these correlations we have created two models to predict the travel time. The first is an empirical model based on our earlier microseism propagation model. The results can be seen in Figure (4). The second model uses a ray theoretic approach which computes how the phase arrivals for a distribution of sources around two stations combine. It calculates the phase delay from the true straight line travel time that will be obtained when computing the travel time from the seismic data. The result can be seen in Figure (5).

Both of our strong correlations show that the travel time fluctuations are indeed a result of the amplitude and the location of the ocean effects near our seismic array. This is evidence to support our HR theory that the microseisms are generated by the interference of the incoming ocean surface waves and the outgoing coastal reflections.

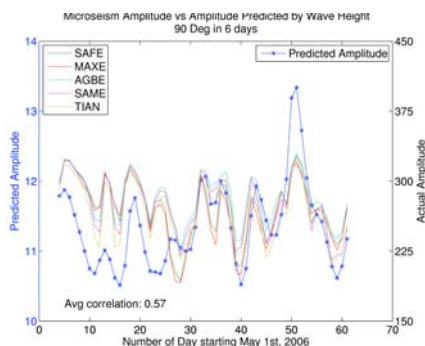


Figure 3 Microseism amplitude computed from the wave height shown with the microseism amplitude computed from the seismic data.

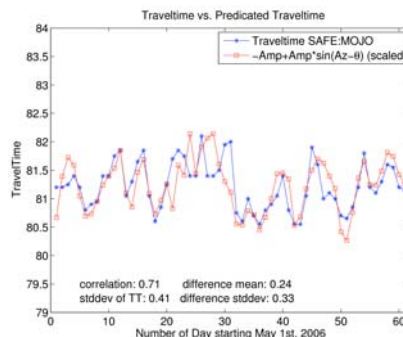


Figure 4 Empirical model used to predict the microseism travel time using the microseism azimuth and amplitude computed from the wave height.

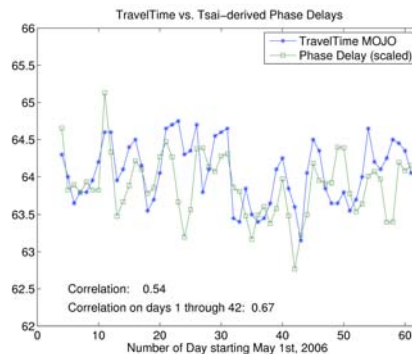


Figure 5 The ray theoretic model used to predict the microseism travel time using the ocean wave height.

### SEI 03.5 Future Directions

The next step is to implement coast reflections in the WAVEWATCH III wave action model software. Since WAVEWATCH III does not implement coast reflection we used the wave height as an approximation in our work. If successful the implementation will provide stronger correlations and more evident to support the HR theory. Other next steps include performing the same analysis with more of the MASE data, data from our Peru Subduction Experiment, and data from other board band seismic stations around the work.

## SEI 04 Scattering of seismic waves by the bathymetry of the trench off Mexico seen in MASE data by applying the Hough transform

### SEI 04.1 Overview

The Middle American Seismic Experiment (MASE) is an interdisciplinary project target to image the subduction of the Cocos plate beneath North America by interconnecting seismic sensor using wireless technologies developed at CENS. The Middle American region raises several questions about the formation of volcanic arcs, water release from the subducting slab and tectonic consequences of this process. The main goal of this experiment is to improve our knowledge on subduction zones by obtaining a high resolution map of the slab, crust and upper mantle. Previous studies in this area were limited by the sparse instrumentation and low resolution velocity models. Nevertheless, data obtained from the MASE experiment has led to new questions about the influence of the topography in the wave propagation and how changes in the propagation medium can be induced excite a particular interface and generate secondary fields.



Figure 1 Location of the MASE seismic stations along Mexico perpendicular to the trench.

Signal processing of the seismic records revealed a strong excitation of scattered waves by the trench caused by the incidence of body waves from teleseismic events. The Pacific trench of Mexico is a submerged structure (Figure 1) located about 30 km from the coast and at a depth of 5km below the sea level. The trench also marks the surface expression of the contact zone between the dense oceanic crust and the lighter continental crust. Our project focuses primarily in analyzing the interaction between the trench and seismic waves coming from events in the Southern Hemisphere. This phenomenon is known in physics as scattering, and occurs when waves encounter obstacles whose size is comparable to their wavelength.

We are approaching this problem from a pattern recognition point of view. Using image processing techniques such as the Hough Transform; we were able to identify, track and isolate the scattered field produced by the trench.

### SEI 04.2 Approach

As mentioned in the previous section, the basic condition for scattering is the size of the wavelength. For teleseismic events (distance > 10,000km), the wavelength of the incident body waves when it reaches the Pacific trench of Mexico ranges between 60-100km, comparable to the structure formed by the trench, the continental crust and the subducting slab. A necessary condition for detecting this signal is sufficient strength of the generating wave. We analyzed events with magnitude larger than 7.0 to obtain a sufficient signal to noise ratio. Finally we assume that both the incident and the scattered wavefront appear as linear traces in the seismic record.

Detection of scattered fields faces several obstacles. First of all, the generating field usually overlaps the scattered field, especially for large events ( $M_w > 7.0$ ) that have a long time function. Another difficulty is the conversion amplitude. The amplitude of the scattered field usually does not exceed the amplitude of the incident field. This makes the signal difficult to detect under noisy environments. Finally, due to failure in the communication system of the stations, bad weather conditions (flooding) and/or urban noise some records could not be either retrieved or used. However, representing the seismograms as color images and applying image processing techniques turns out to be an efficient way to overcome all these difficulties.

### SEI 04.3 System Description and Experiments

The Middle American Seismic Experiment is a joint international project that involved CENS/UCLA, Caltech and the National Autonomous University of Mexico. This high density network was installed in 2005 and pulled out in 2007 providing two years of high resolution data of the area. The array consisted of 100 broadband seismic stations extended for almost 550km from the city of Acapulco towards the North, to the city of Temporal only 80km away from

the coast of the Gulf of Mexico. 50 of these stations functioned as standalone stations requiring manual data retrieving at monthly basis. The remaining 50 stations, managed by CENS/UCLA, collected data and broadcasted wirelessly at daily basis to a central computer in Mexico City, for its later retransmission through a regular internet connection to the central database in Caltech, Pasadena. Linear layout (perpendicular to the trench), high spatial density (every 5km) and high sensitivity equipment (Guralp CMG-3T with a sampling rate of 100Hz) of this network resulted in one of the most advance portable arrays around the globe.

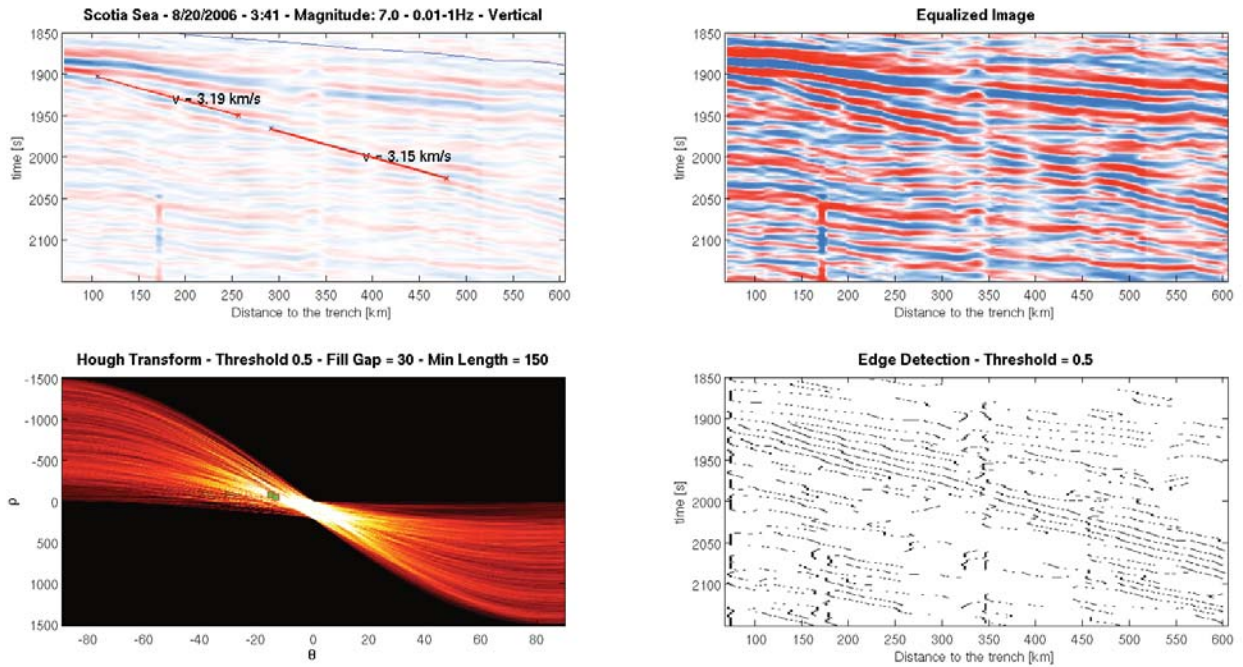


Figure 2. Top left - Pseudo-color image of the data obtained by interpolating seismograms; red indicates a positive velocity whereas blue shows negative values. Top Right – Equalized image. Bottom Right – Edge detection performed using an edge detector with threshold of 0.5. Left bottom. Hough transform representation of the edge map.  $\theta$  axis is the slope in degrees of all possible lines crossing a every pixel labeled as edge; and  $\rho$  axis is the distance to the origin in pixels; the green square shows the points where curves converges (Note. The bright spot at  $\theta=0$  corresponds to the trivial solution and therefore is ruled out).

We analyze data from this array for seven events with magnitude larger than 7.0 shown in Table 1. Data from individual stations were combined into a single matrix using a regular grid in time and space. Representation of the data as a matrix made the visualization easier and the use of image processing techniques possible. Missing data was estimated by interpolating records from neighboring stations to obtain a continuous representation. We started the processing of the image by first equalizing the seismic records. Afterwards, we apply an edge detector to mark possible phases in the record. Finally, we look for linear patterns in the edge map using the Hough Transform. This transformation can be briefly described as a map in the parameter space of all possible lines than can be traced through a specific point in space. Once every point in the edge map is associated with a family of lines in the parameter space, we inspect the areas where the density of curves is higher and consequently represents a pair of parameters corresponding to a line marking the arrival of either the incident or scattered field. We constrained the

Date	Region	Latitude	Longitude	Depth	Magnitude	Distance	Backazimuth
2006/01/02	Sandwich I.	-60.96	-21.61	13	7.4	99.16	151.23
2006/01/02	Fiji I.	-19.93	-178.18	582	7.2	85.24	247.50
2006/05/03	Tonga	-20.19	-174.12	55	8.0	81.76	245.90
2006/05/16	Kermadec I.	-31.81	-179.31	152	7.4	90.25	236.67
2006/07/17	Scotia Sea	-61.03	-34.37	13	7.0	93.54	153.80
2007/03/25	Vanuatu	-20.62	-169.36	34	7.1	96.58	250.40
2007/04/01	Solomon I.	-8.47	157.04	24	8.1	104.95	262.50

Table 1 Detection of the scattered field was successfully achieved for seven events at teleseismic distances > 10,000km during the time of the experiment. Table shows their location magnitude and time of the event.

solutions by assuming that the scattered phases travel at a surface wave speed (between 3-4 km/s), this process allows us to discriminate between scattered body waves and scattered surface waves from the trench. The Hough transform turned out to be an efficient tool to detect scattered signals from the trench despite the noisy environment and the missing data.

Once the scattered field has been detected, it is now possible to formulate new hypotheses about the possible mechanism that determine this phenomenon. So far, we have shown that the scattered field branches off from incident low frequency body waves when the body waves from teleseismic events cross the trench. The velocity of the scattered field propagating through the array suggests that part of the energy from the incident body waves is converted into surface waves. However, how this process occurs and what factors determine the conversion is still an open question and will be explored in future work.

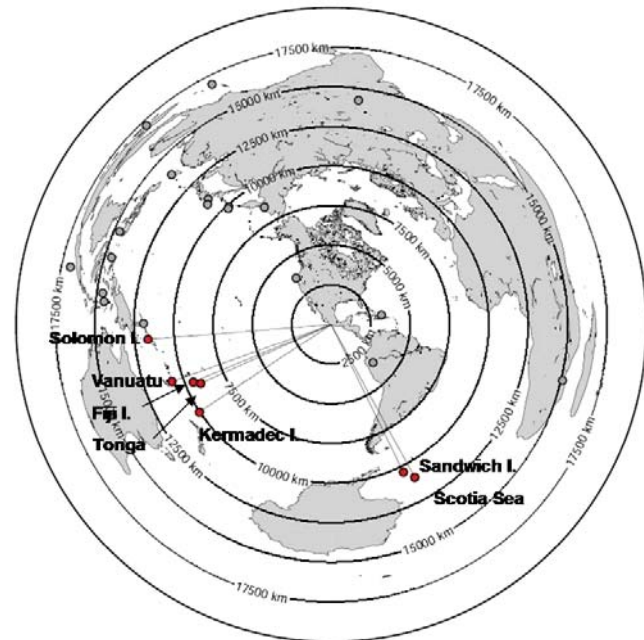
#### SEI 04.4 Accomplishments

Despite of the overlapping of the scattered field by the incident body waves, and the low signal to noise ratio that seemed to make the scattered field, in many of the cases, virtually invisible. We successfully identified scattered phases for seven events due to interaction of body waves and the Pacific trench of Mexico. Fig. 3, shows the location of these events. We identify some of the ingredients needed to induce scattering at the trench: (1) Distance from the array; for all cases a minimum distance of 10,000km is required in order to bias the spectrum of the incident field towards long wavelengths comparable to the size of the trench and the subduction zone; (2) Magnitude; only events with  $M_w > 7.0$  caused a field strong enough to be detectable by the network; (3) incident angle; all events analyzed shown an oblique incidence to the trench. This condition is constrained by the distribution of earthquakes during the time of the experiment. Further investigation is required to confirm or rule out this constraint.

This result is critically important for studies imaging the crust and upper mantle. When the MASE network was installed in 2005, the main goal was to obtain a high resolution image of the subducting slab beneath Mexico. However, parasitic signals such as scattered phases from the trench might lead to erroneous interpretation of the results. Correcting, modeling and detecting of the scattered field provides a new application of the network from its original target. Understanding scattered fields at topographic scales is important not only for removing an undesired signal from the seismic records, but also might shed light into the factors that can cause site effect resonance and amplification.

#### SEI 04.5 Future Directions

Results obtained by applying the Hough Transform to the synthetic seismograms revealed a new tool to identify phases through the MASE array. Three major directions of research are now needed it. (1) Apply this technique to other events at different wavelength intervals to seek for other possible scatters such as volcanic arcs, mountain ranges, basins, etc. (2) to develop a more general technique to track and detect non linear phases such as the Radon transform. The major disadvantage of this technique is that it is only applicable to phases with a linear move-out which is only valid when very long structures such as a trench cause radiation of the scattered wavefield. For smaller structures this may not be the case. Therefore a more general technique is need it. (3) Modeling. To prove the identification of the scattered wavefield requires a mathematical model that explains the physics behind this effect. Several techniques such as the spectral element method, the indirect boundary element method or finite frequency analysis can be used to solve the wave equation for different geometries and media. Understanding the effect produced by heterogeneities in the medium and/or irregularities in the topography will provide a better picture of site effects and more accurate hazard maps.



Events  $M_w > 7.0$  from 2005/01/01 through 2007/07/01  
 Figure 3. Azimuthal map of events with magnitude larger than  $M_w 7.0$  recorded by the MASE network. Red dots shown events that reveal induced by body waves crossing the trench.

## SEI 05 GeoNet: A Platform for Rapid Distributed Geophysical Sensing

### SEI 05.1 Overview

- We co-convened an IRIS (Incorporated Research Institutions for Seismology) workshop on FlexiRAMP at the meeting of the Seismological Society of America Annual meeting in 2009. (FlexiRAMP is a flexible array of rapidly deployed seismic stations in aftershock zones or elsewhere using Rapid Array Mobilization Procedure)
- After multiple meetings during the year we took delivery of two GeoNet nodes constructed by Reftek.
- We added the UCLA LEAP (Low Energy Aware Processors) board modules to the GeoNet boxes.
- Field tests of the new integrated GeoNet Boxes have been undertaken.

The idea of a CENS Emsbox was first floated at our Palm Spring retreat in the third year of CENS. It is now gratifying to have the first units delivered for testing. The Emsboxes that for seismologic purposes we refer to as GeoNet are a collaborative design from UCLA groups in Electrical Engineering, Computer Science, Structural Engineering and Earth and Space Sciences.

### SEI 05.2 Approach

The science objectives are to use a rapidly installable wirelessly linked seismic network to measure earthquake or volcano sources in the near field to understand the underlying physics, or in buildings to understand earthquake damage. Low power is the key to rapid installation. To accomplish these objectives, we collaborated with Reftek to construct a new generation digital acquisition system (DAS) based on the CENS-developed LEAP (low-power energy aware processing) system and a newly developed low-power A/D converter from Texas Instruments (TI) that became recently available.

During this year of GeoNet, one of the leading manufacturers of seismic recording systems, Refraction Technology, Dallas Texas, or Reftek, constructed several prototypes. They will be extensively tested in a field environment during a number of deployments.

In preparation for GeoNet, we have used the Mexico and Peru networks to test the software including improving Disruption Tolerant Shell (DTS), measurement of radio link quality (ETT), network logging, an embedded web interface based on Emstar for deployment and maintenance, network timing, a new routing protocol that caches the routes across sleep cycles for a fast startup. The Peru network has been installed for over a year and we can add to it GeoNet nodes for further testing and debugging.

We used the Mexico and Peru networks as testbeds for GeoNet systems software research. In anticipation of the GeoNet prototypes, a number of advancements have been made to the software system during the recent seismic deployment.

The field objective is to have only two separate parts: DAS and a seismic sensor. The DAS would have a solar panel attached on top, battery inside (with external power plug), internal GPS antenna (with a possibility attaching an external one), external N-type connector to attach an antenna. Field installation would involve attaching the box to a post and bury the seismometer (figure 1). It would then be a node in a wireless network of neighbors, e.g. along a dirt road that could bring event data out in real time, or, in the low power mode, on a duty cycle, e.g., 5 min every hour. The radios would also deliver network time, a backup to GPS.

In a building, the instrument would not need the solar panels, although after an earthquake power may be unavailable. Instrument plus Episensor (or other) would be installed on various floors. Radio connectivity through the floors would be used to provide network time (essential) and transport event data. Where available (e.g., near windows) GPS time would calibrate network time. With no solar, the battery with an active sensor would last 4 days. Longer deployments would require a larger external battery.

We therefore suggested that in the spirit of the highly successful RefTek Texan instrument the GeoNet be 3 or 6 channels, have internal 12AH lead acid battery, internal GPS antenna with external plug as an alternative, passive instrument A/D interface (and/or Episensor interface), internal 802.11 radio with external antenna plug, external LEDs to signify functions (or LCD), attached external flash compartment, GPS and network time stamps with 0.1 ppm time precision, external sensor conditioner control-box for active sensors, Linux operating system, LEAP computer with sleep-wake modes compatible with CENS networking software, brick type enclosure (to allow stacking) with lip around plugs for protection, and screw holes for attached solar panel. External serial and ethernet/USB plugs.

Reftek delivered two prototypes in October 2009:

The software design for the seismological community will include CENS networking auto routing component and the low power configuration ability of the hardware. To conserve power the processor will duty cycle between sleep and wake states.

The node is based on the Linux operating system, with 802.11 capabilities for wireless networking. Software development is required for array-event detect, network and GPS timing, multi-hopping the data, and near real-time data analysis and modeling. The software system will be based on the infrastructure used in the Peru network. However, the existing software system is not directly applicable because of a number of factors introduced by the application requirements. These include duty cycling, non linear network topologies, array event detect, and the time span of the deployments. We are developing software to deal with these new factors, in particular: sleep schedule aware data delivery, disk space based routing, deployment tools, and integration with Wavescope to enable streaming, network processing, and cooperative event detection.

In preparation for the Peru seismic deployment, we have improved the Disruption Tolerant Shell (DTS) system used in the Mexico seismic deployment. In particular, we improved the efficiency of the underlying network service called statesync, lowering the total amount of traffic generated by DTS. Also, the routing protocol is improved to detect and eliminate routing loops.

We developed a new link quality estimation component for use in our deployments. Our previous link quality estimators were based on the ETX (expected number of transmissions) metric. While ETX worked well for our seismic and acoustic deployments, there were some issues with the stability and accuracy of the metric, which can be improved. These issues are well known and are solved with the ETT (expected transmission time) metric. The new component is being used in the Peru seismic deployment.

Network time synchronization has been well researched as a service. However, over the years we have discovered that having a network time synchronization service is often not enough. Disruptions in the network, faults in nodes, and startup time can cause the network time synchronization service to not

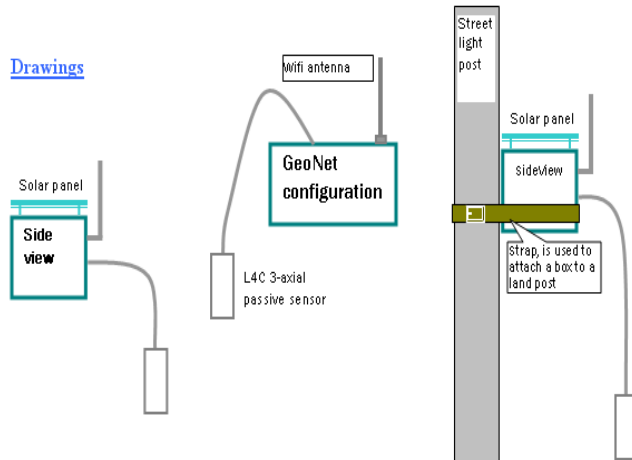


Figure 1: Schematics of possible field installations



Fig.2. A prototype of the GeoNet box with modular approach inside

always be on. In that case, the system misses events or possibly results in incorrectly synchronized data. In the seismic deployments, the hardware used was able to properly timestamp the seismic data; however system logs and status were always based on node system time, which would be reset after a reboot.

We created a component, which addresses this problem for the Peru deployment and provides a framework for more robust time synchronization implementations in the future. It provides the ability to use multiple time synchronization services, each with different accuracies, overheads, and startup times. It also adds meta-data about the time synchronization protocol in uses and its estimated accuracy. Our first implementation of the enhanced time synchronization service is called Timekeeper and is being used in the seismic Peru deployment. It focuses on maintaining system time so that system log data is correctly time-stamped.

In our previous deployments, there was no persistent log recording system. DTS enabled the viewing of live log data but it did not provide the ability to save all the logs data from the entire network. Since it is impossible for someone to attend to the network all the time, we were unable to observe faults, status, and events through the logs well after they had happened. For this reason, we built a component to collect the logs periodically, compresses them, send them to the central repository using the same data delivery channels as used to seismic data.

We also added a web interface utilizing the existing Emstar web framework to help with site deployment and to make site maintenance visits easier by providing a simple and clear interface to relevant data. In addition, the new web interface can also be used to configure the seismic sensors (Q330).

We began work on adapting the base software system used in Mexico and Peru to GeoNet. GeoNet will be a heavily duty cycled system and the entire software system needs to be aware of the sleep scheduling in particular routing and data delivery. The existing software will probably work, but it will be inefficient causing a loss in the overall amount of data that can be delivered. We began adapting the routing to have a fast startup after a sleep cycle with a fast and reliable route confirmation mechanism. The new routing caches the routes across sleep cycles for a fast startup.

While time synchronization in our software system does work, there were components that were missing and incomplete, for the GeoNet project. These components synchronize an RBS network time with that of a GPS. This is important for GeoNet because the system needs to be aware of the true length of a second to properly record data and enable it to be referenced to external systems.

### **SEI 05.3 System Description and Experiments**

The best experiment for GeoNet is an aftershock deployment, but it could also cover any seismic experiment where rapid deployment is necessary (volcanoes, explosions of opportunity). A pool of identical instruments would be available to either install in buildings or in the field and could be standalone or where appropriate nodes in a wireless network. The objective is to measure strong shaking from the largest aftershock for both science and engineering objectives. The GeoNet/SHM requirements have much in common, but there are differences. Building installations do not have access to GPS time, may or may not have power. Field installations, being remote and widespread, need power. Building sensors tend to be active (Episensor). Field installations can have passive sensors, requiring significantly less power.

### **SEI 05.4 Accomplishments**

The new communication and data collection software was tested and installed on the CENS data communications controllers during the seismic deployment in Peru. A number of posters were presented about different features of system (software and hardware) at the Fall AGU-2009 meeting and Spring SSA meeting, as well as papers published. Igor Stubailo won an outstanding student paper award at the SSA meeting.

### **SEI 05.5 Future Directions**

We will continue working on integrating duty cycling with existing software based used in Mexico and Peru. This includes further developing a robust routing algorithm that can deal with nodes with limited storage space with a complete a centralized method to dynamically schedule duty cycling and transmissions.

We will develop software to deal with sleep schedule aware data delivery, disk space based routing, as well as tools for network processing and cooperative event detection. The GeoNet instruments will have application over a wide range of field applications involving wide area networks and low power processing and delivery of event data. They will run on small batteries with a laptop sized solar panel.

## SEI 06 Towards a multi-tier sensor array for instrumenting large buildings

### SEI 06.1 Overview

Structural Health Monitoring (SHM) has important applications in fields like civil engineering and seismology. The emergence of wireless sensor networks (WSN) provides a promising means to such applications. However, while most WSNs are in the experimentation stage, very few take into consideration realistic application requirements. To collect comprehensive data for SHM domain experts, high-resolution vibration sensors and sufficient sampling rates should be adopted. This makes it challenging for current WSN technology in the following aspects: processing capabilities, storage limit, and communication bandwidth. The wireless sensor network has to meet expectations set by wired sensor devices prevalent in the structural health monitoring community. In this project, we are building an application-realistic portable wireless sensor network called ShakeNet for instrumentation of large civil structures, particularly buildings or bridges after earthquakes. ShakeNet will be easily deployable by 2-3 people within hours after an earthquake in order to measure the structural response of the building or bridge using aftershock recordings. ShakeNet involves the development of a state-of-the-art sensing platform (ShakeBox), and installation and execution of the Tenet software suite for networking, data collection and monitoring.

### SEI 06.2 Approach

ShakeNet is motivated by our work on instrumenting a long-span suspension bridge, the Vincent Thomas Bridge at the entrance to the Los Angeles Harbor, with wireless sensors. For the experiment twenty wireless sensors were deployed on the bridge, and the sensor network acquired vibration samples continuously from each sensor for 24 hours. The results from the experiment were encouraging; deployments were done in a matter of hours, and the structural characteristics derived from the collected data were consistent with previously published results. However, a few shortcomings were highlighted; the MDA-400 vibration card with 16-bit ADC that was used for recording the vibrations was not suitable for capturing low (< 1Hz) fundamental frequencies of large structures. As the structure size increases we generally observe lower fundamental frequencies of vibration which are of interest for structural monitoring and analysis. In addition, the development and preparation time required off-site prior to deployment was substantial.

Although we were able to extract macroscopic structural properties such as the modal frequencies, the board (the MDA-400 from Crossbow) that we used had several shortcomings. It has only 16-bit resolution; as we show below, this resolution is inadequate for monitoring ambient vibrations in large structures. It was originally designed for high-frequency sensing in the KHz range, so its response in the sub-1Hz modal frequency range of large structures is poor. It had a hardware fault which resulted in a signal offset that caused signal clipping at high amplitudes. Finally, the board was designed to interface only with a limited set of accelerometers, none of which was perfectly suited for structural sensing. A better accelerometer with higher signal-to-noise-ratio and sensitivity was needed for structural health monitoring. We addressed these issues while developing the ShakeBox for ShakeNet.

ShakeNet deployment would have required placing the nodes in a harsh radio environment. It requires the communication protocol to take care of packet drops and finding a route to the sink. Development of robust and working protocols for these operations from scratch requires considerable time and expertise. We do not envision the end users for ShakeNet to write WSN data collection and communication protocols. Use of an existing WSN software and modification for ShakeNet requirements reduces the development time. We also need a WSN which can be tasked to operate a number of applications. It should also have tools which can help in rapid application development and changes to them, as well as for rapid deployment in field. Tenet fulfills a number of these requirements and hence has been used to develop the software suite required to run ShakeNet over ShakeBoxes.

### SEI 06.3 System(s) Description and/or Experiments

#### *ShakeBox Description*

In collaboration with Refraction Technologies Inc. of Plano, TX, we are adopting a modular design paradigm for the ShakeBox (Figure 1, left), which consists of four independent modules: CPU, Power, Analog to Digital (A/D) and Sensor, connected via standard SPI protocol. Figure 1 (right) shows the CPU, Power and A/D modules. These modules are then housed in a custom made weather-proof casing as shown in Figure 1 (left). Below is a short description of the different modules of ShakeBox and the associated characteristics.

#### *CPU Module*

The CPU module contains the system processor (a Crossbow iMote2 mote) and the RT617 board and controls all system operations. The iMote2 mote controls the communication to the other three modules via two SPI interfaces. The RT617 board consists of FPGA, precision oscillator, battery backed RTC, SD memory card slot, GPS interface and a board ID EEPROMs. It also provides the timing for Power and A/D modules. iMote2 is an advanced sensor network platform and consists of a PXA271A 32bit microcontroller and CC2420 radio. It has multiple communication

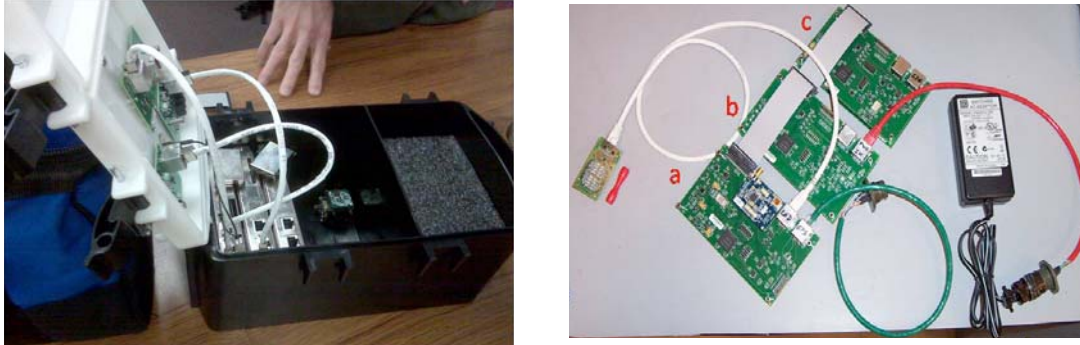


Figure 4. ShakeBox with weather-proof enclosure (left) and detailed modules (right): a) CPU module with iMote2, b) power module, and c) A/D module.

interfaces; prominent among these are the SPI, I2C, USB host and USB slave, JTAG and AC97 audio codec. CC2420 is an 802.15.4 compliant 2.4GHz radio which can give up to 256Kbps bit rate. Dynamic scaling of core frequency of the PAX271 microcontroller from 13MHz to 208MHz provides a varied range of options for balancing processing power with energy usage.

#### *Power Module*

The Power module provides the power requirements of the different components and consists of RT618 FPGA board and RT620 power board. RT618 provides communication with the CPU module, a clock, control of the voltage monitor A/D converter, control of analog power supplies and board ID EEPROMs. RT620 provides an input power controller, switching supplies at different voltage levels, a 16-bit A/D monitor for supply voltages and input currents, and a board ID EEPROMs.

#### *Analog to Digital Module*

The A/D module takes the analog sensor inputs and provides a time-stamped 24-bit digital output, and consists of RT618 FPGA board and RT614 analog board. RT618 provides communication with CPU module, a clock for time stamping sampling data, control of A/D chips, test-signal generator for debugging, relay control, a board ID EEPROMs and sensor ID interface. RT614 provides the scaling of sensor signal voltages, three 24-bit A/D converters, replays to connect test signals to internal analog inputs, a board ID EEPROMs and voltage regulators.

#### *Sensing Module*

The sensor module consists of three Colibrys SiFlex 1500 accelerometers which are interfaced to the RT614 board in the A/D module. The SiFlex1500 operates from a bipolar power supply voltage that can range from  $\pm 6V$  to  $\pm 15V$  with a typical current consumption of 12mA at  $\pm 6V$ . The linear full acceleration range is  $\pm 3g$  with a corresponding sensitivity of 1.2V/g.

#### *Weather-proof Casing*

The weatherproof casing houses all the modules. Each module is electronically shielded to protect against electromagnetic disturbance. The lead acid battery used in the ShakeBox is placed in a separate sealed compartment to isolate it from the electronics in case of battery leakage. The box provides serial connectors, a connector for GPS, LEDs for display and feedback, and antenna connector for a high-gain external antenna used by the iMote2 radio. It has three screws and a spirit level for leveling. The prototype box in Figure 1 is made up of resin plastic but the production pieces will be metallic aluminum.

#### *Communication*

Communication between modules in ShakeBox is achieved via three buses: the SEL bus, the SPI command and control bus, and the AD data bus. While the SEL bus is used by the iMote2 mote to select a specific component in a module, the SPI command and control bus (the SPI1 port on iMote2) is used to communicate with that component. The AD data bus (the SPI2 port on iMote2) is used for the iMote2 mote to collect sampling data from A/D module and auxiliary data from the Power module. During development we will need debugging facility and features to upload driver code and FPGA images on the boards. The board modules expose the JTAG port for FPGA programming while iMote2 is programmed and debugged using the USB slave port.

#### *Tenet*

The software for running ShakeNet has been built using the Tenet architecture. Tenet is based on the observation that for scalability, today's sensor network deployments ideally have two tiers: a lower tier consisting of motes which enable flexible deployment of dense instrumentation, and an upper tier containing fewer, relatively less-constrained 32-bit nodes with higher-bandwidth radios, which we call masters. Tenet constrains the placement of application

functionality in a sensor network according to the following Tenet Principle: Multi-node data fusion functionality and multi-node application logic should be implemented only in the master tier. The cost and complexity of implementing this functionality in a fully distributed fashion on motes outweighs the performance benefits of doing so. Since the computation and storage capabilities of masters are likely to be at least an order of magnitude higher than the motes at any point in the technology curve, masters are the more natural candidates for data fusion. The principle does allow motes to process locally-generated sensor data, and can result in significant communication energy savings. Over the period of the project we have been able to port the Tenet software suite for running over imote2 (the mote used for ShakeBox) and add additional features to be able to run ShakeNet.

#### *Function generator test*

From May to June 2009, we carried out a series of experiments to test the accuracy of the ADC in ShakeBox. The equipment we used was a HP33120A Function Generator which accepts user-defined parameters to generate an analog wave signal. We fed it to the ShakeBox, collected the response from the ADC and analyzed the resulting FFT, coherence, and cross-correlation between channels. We varied the frequency range from 0.2 to 125 Hz which covers significant frequencies in earthquake engineering analyses, and the amplitude ranged from 1 to 19 Vpp. We also measured the noise characteristics of each ADC channel, with and without function generator connected. Due to space limitation, we only present one set of results here: frequency sweep from 0.2 to 125 Hz with 1Vpp amplitude. For more details, please refer to <http://enl.usc.edu/enlwiki/ShakeNetTestResultLatest>.

Figure 2 shows the FFT analysis for a frequency sweep from 0.2 to 125 Hz. We can see that the ADC has a reasonable response until around 100 Hz, above which the response drops dramatically from 100 to 125 Hz. This is expected behavior according to the ADC datasheet.

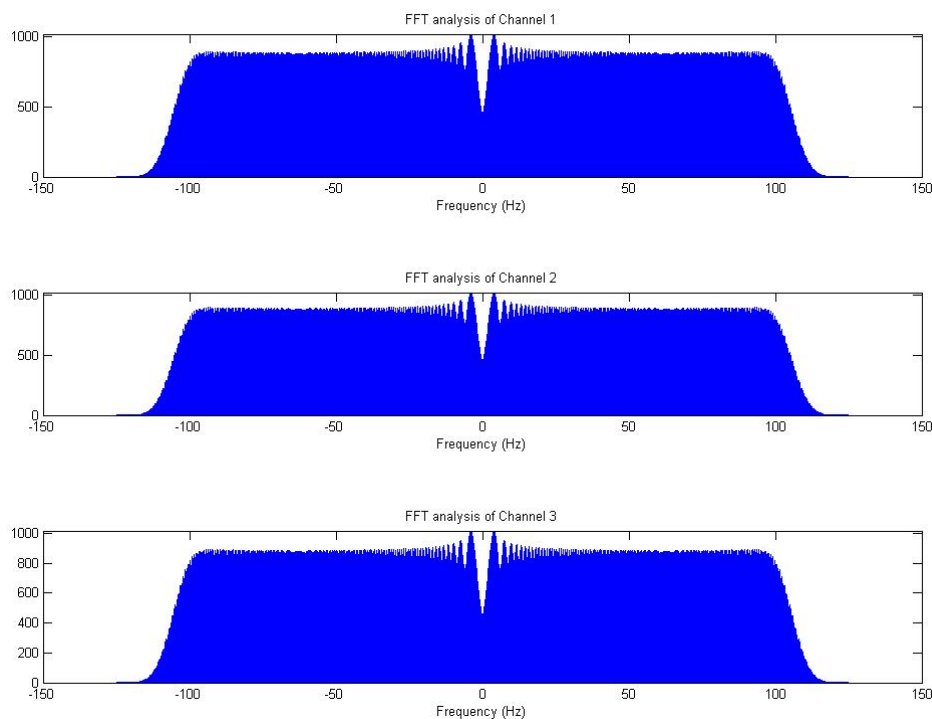


Figure 5. FFT analysis for frequency sweep 0.2-125 Hz with 1 Vpp amplitude

#### *Shake table test*

In July 2009, we conducted an electrodynamic shake table test in the Dept. of Civil Engineering at Caltech. The shake table input was fixed at frequencies between 0.1 and 90.0 Hz, and the ShakeBox response was compared with colocated Dytran piezoelectric accelerometers. Figure 3 shows the shake table test equipment and set up.

We ran the unidirectional shaker at 0.1, 0.5, 0.8, 1.0, 1.5, 1.2, 2.0, 5.0, 10.0, 25.0, 49.0, 50.0, and 90.0 Hz for between 10 seconds and two minutes using a sinusoidal wave as input. A two-minute ambient vibration test was conducted at the end of the test. Nine Dytran accelerometers were attached to the sides and top of a mounting plate (three in each direction). These were connected to a 24-bit Granite digitizer with GPS receiver. The Dytrons have flat

response for 1-2000 Hz with a range of  $\pm 50$  g, and were calibrated at the factory in early 2009. During the tests, we compared the Dytran-Granite vs. ShakeBox performance in near-real time and observed close similarities in waveform shape and amplitudes. Though the input was a sine wave, the shaker appeared to give a little kick at each end of its travel distance. This produced additional peaks in the output seen on both the Dytrons and Colibrays sensors. Since we observed the response to these kicks on both sets of accelerometers, we concluded that it was not due to a fault in accelerometer response. Even though the channels were lined up parallel to and perpendicular to the direction of shaker motion (Figure 3 Left and Middle), the motion was not perfectly 1D, so a response was also observed in the other orthogonal channels but at lower amplitudes. Dytran-Granite timing was based on GPS time stamps and the ShakeBox timing was based on board time stamps with the PC clock, so Dytran-Granite timing was used as the reference start time.

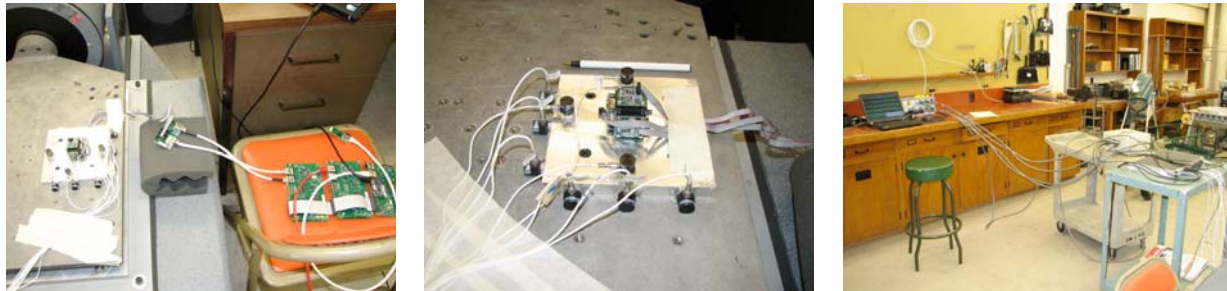


Figure 3. Left: Shake table top showing mounted steel plate with Dytran piezoelectric and Colibrays MEMS accelerometers and additional ShakeBox components on chair. Middle: Closeup of mounted plate with accelerometers. Right: 24-bit digitizer and PC recording setup for Dytran accelerometers.

For each frequency test we compared waveform shapes between Dytran-Granite and ShakeBox performance, expecting differences to be indications of questionable or faulty performance. Examination of absolute amplitudes showed that they were within 10% or better of each other, indicating good ShakeBox performance (Figure 4). The observed spectral peaks in the FFTs computed from the acceleration time series of both types of sensors also showed good agreement between the two systems.

#### Millikan library test

In October 2009, we conducted a ShakeBox performance test at the Millikan Library on the Caltech campus. The objective was to compare the ShakeBox performance vs. the permanent Episensor accelerometer performance

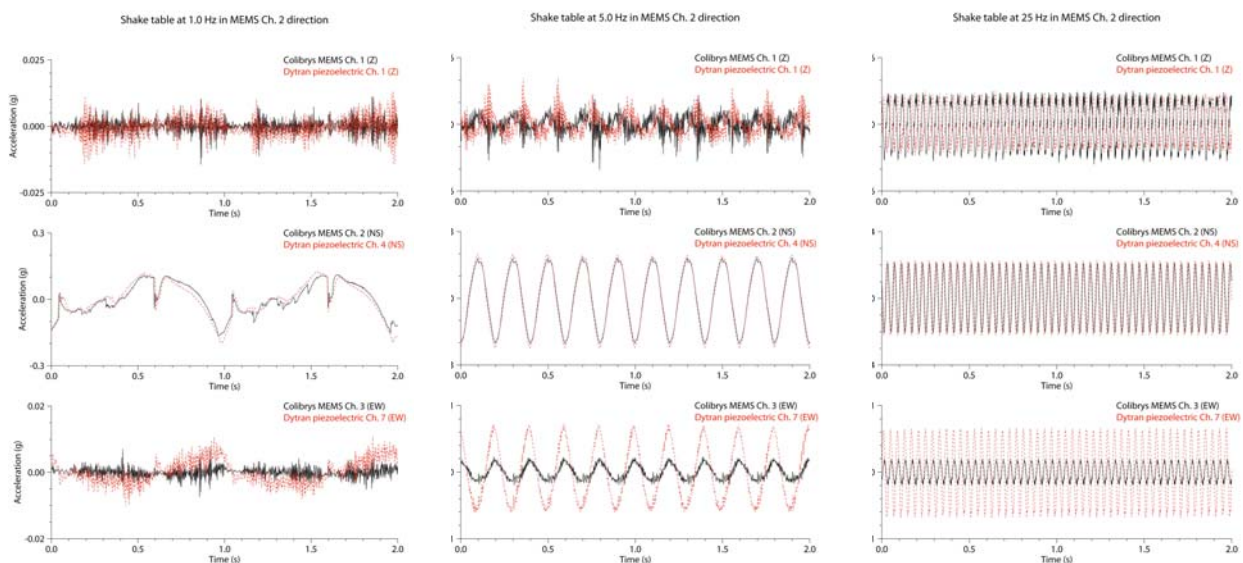


Figure 4. Shake table test results comparing ShakeBox (Colibrays MEMS: black curves) with Dytran piezoelectric accelerometer response (red curves), recorded at 100 sps. Left: 1 Hz sine wave input. Middle: 5 Hz input. Right: 25 Hz input.

during several forced vibration tests. The Episensor is a broadband force-balance accelerometer used in permanent wired structural arrays and has reliable, low-noise performance. An eccentric mass shaker is located on the Millikan Library roof and provided the excitation in a single horizontal direction at a time. Two Shakeboxes were colocated with three-component Episensor accelerometers in Millikan Library on the 9th floor and in the basement. Millikan Library is a 9-story reinforced concrete building consisting of both shear walls and moment frames. Shear walls dominate the east and west faces of the building and also line the elevator core in the center of the building. The shaker was run at frequencies between 1.0 Hz and 9.5 Hz and each ShakeBox response was compared with the colocated Episensor accelerometers.

The forced vibration tests consisted of an initial empty-buckets test (no weights added, resulting in minimum applied force), a full-buckets test (all weights added resulting in maximum applied force) in the east-west direction, and a full-buckets test in the north-south direction. The empty-buckets shake spanned frequencies from 1.0 to 9.5 Hz gradually over the course of approximately 40 minutes. The rate changed over the course of the sweep. The lower frequencies progressed at 0.05 Hz intervals every 20 seconds, from 2.5 Hz to 5 Hz progressing at 0.05 Hz intervals every 15 seconds, and from 5 Hz to 9.5 Hz progressing at 0.05 Hz intervals every 10 seconds. This frequency range covers the building's first EW modal frequency of 1.2 Hz (ambient), the first NS mode frequency of 1.7 Hz (ambient) and the first torsional mode frequency of 2.4 Hz (ambient). The second test consisted of a full-buckets shake (full set of weights for increased force resulting in temporary nonlinear response) for frequencies between 1.0 Hz and 2.5 Hz, particularly to excite the first EW frequency at 1.15 Hz (nonlinear response due to full set of weights). The sweep up to 2.5 Hz and back down to the starting frequency of 1.0 Hz took approximately 30 minutes. The EW full-buckets test also excited the torsional mode (2.3 Hz, nonlinear) in a narrow band around the mode progressing at a rate of 0.2 Hz intervals every 45 sec. At the end of this test we paused near the peak resonance for around a minute at both the first EW and torsional mode frequencies. The first EW frequency shake shows up primarily in the EW components of the accelerometers, and the first torsional shake shows up very clearly in both the EW and NS components. The third test consisted of a full-buckets frequency sweep in the NS direction for frequencies between 1.0 Hz and 1.8 Hz, particularly to excite the first NS frequency at 1.6 Hz (nonlinear). The NS full-buckets test excited the first NS frequency in a narrow band around the mode progressing at a rate of 0.2 Hz intervals every 45 sec. At the end of the test we paused again at resonance on our way back to 0 Hz. As the shaker frequency intersected these modes we got increased response resulting in increased amplitudes.

The recorded accelerations for both types instruments in the Basement and 9th floor locations are shown in Figure 5, plotted in the same comparable units (milli-g). Note that the amplitude scales are different for each component.

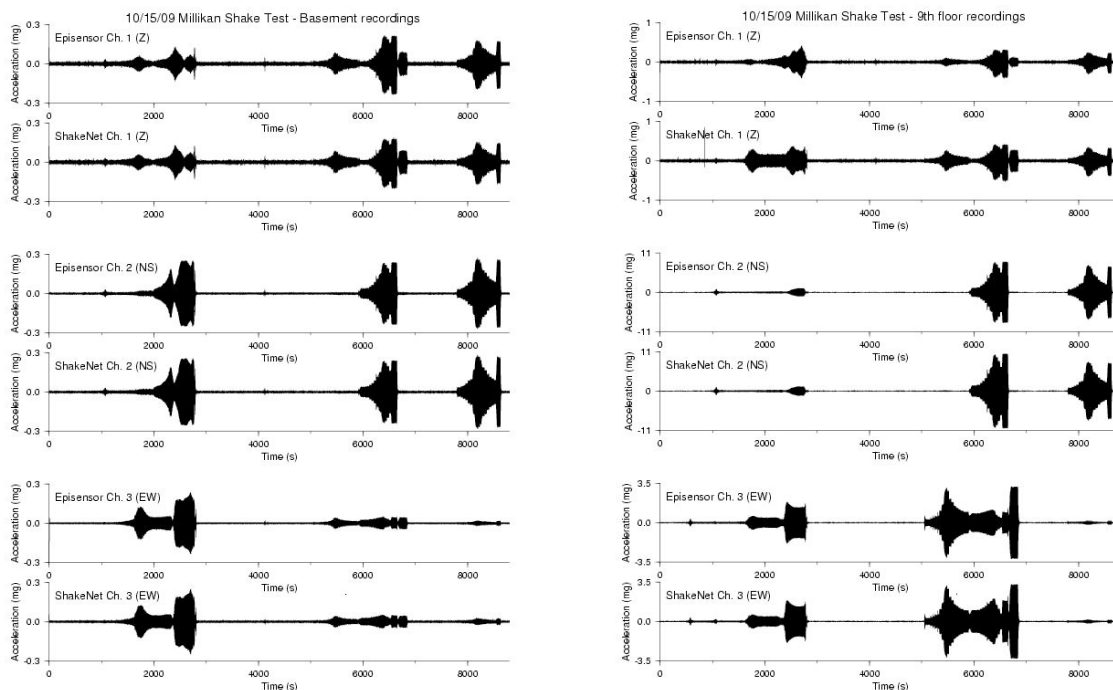


Figure 5. Acceleration responses due to forced vibrations recorded by the ShakeBoxes colocated with Episensors in the Basement (Left) and on the 9th floor of Millikan Library (Right).

Overall the response of the ShakeBox-Colibrys is quite similar to that of the Episensor-Granite except that the ShakeBox amplitudes are usually about 10-20% larger. This may be due to the lack of robust physical coupling of the ShakeBox with the floor slab in both locations (we placed our boxes on the floor whereas the Episensors are bolted into floor slabs or walls). In fact the amplitude difference is larger at the 9th floor where the shaking was stronger than in the basement.

#### **SEI 06.4 Accomplishments**

We have built a working sensing system - the ShakeBox, including both hardware boards and Tenet software tool suite.

We have conducted a series of experiments as described in section 3.

#### **SEI 06.5 Future Directions**

ShakeNet data collection happens using the Tenet hierarchical architecture. We have a higher tier of master nodes which task the nodes and collect the data responses coming from them. The current prototype is able to collect data from two ShakeBoxes sampling data at 125 Hz under each master. At this point we saturate the available radio bandwidth and hence cannot add anymore ShakeBoxes under this master. To overcome this limitation, we are implementing the Steim2 algorithm for compressing data on each ShakeBox prior to sending it to the master.

Time synchronization is required for correlation of data collected across ShakeBoxes. Since the ShakeBoxes will be placed inside the building or structure, using GPS for time synchronization cannot be counted on. We use network time synchronization over the mote and master cloud. Currently we use network time protocol (NTP) for master cloud time synchronization and Flooding Time Synchronization Protocol (FTSP) for time synchronization over the mote cloud. We are developing a method to time-synchronize the mote and master cloud over USB. This becomes challenging due to the requirement of only a few millisecond error margin for time synchronization imposed by domain experts.

After the integration test of the system as a whole, we plan to deploy 40 ShakeBoxes in realistic environments, for example, the Factor building at UCLA, the Santa Ana River Bridge and the Seven Oaks Dam. We will test the working flow of the whole system and the fidelity of the sampling data collected.